Nanomanufacturing and Metrology (2024) 7:1
https://doi.org/10.1007/s41871-024-00222-z

ORIGINAL ARTICLE

Fabrication of Superhydrophobic–Hydrophilic Patterned Cu@Ag Composite SERS Substrate via Femtosecond Laser

Yuheng Zhang[1] · Zongwei Xu[1] · Kun Zhang[2] · Ying Song[1] · Bing Dong[1] · Jianshi Wang[1] · Mengzhi Yan[1] · Qingqing Sun[1]

Received: 19 November 2023 / Revised: 2 January 2024 / Accepted: 4 January 2024

Abstract

Ultralow concentration molecular detection is critical in various fields, e.g., food safety, environmental monitoring, and disease diagnosis. Highly sensitive surface-enhanced Raman scattering (SERS) based on ultra-wettable surfaces has attracted attention due to its unique ability to detect trace molecules. However, the complexity and cost associated with the preparation of traditional SERS substrates restrict their practical application. Thus, an efficient SERS substrate preparation with high sensitivity, a simplified process, and controllable cost is required. In this study, a superhydrophobic–hydrophilic patterned Cu@Ag composite SERS substrate was fabricated using femtosecond laser processing technology combined with silver plating and surface modification treatment. By inducing periodic stripe structures through femtosecond laser processing, the developed substrate achieves uniform distribution hotspots. Using the surface wettability difference, the object to be measured can be confined in the hydrophilic region and the edge of the hydrophilic region, where the analyte is enriched by the coffee ring effect, can be quickly located by surface morphology difference of micro-nanostructures; thus, greatly improving detection efficiency. The fabricated SERS substrate can detect Rhodamine 6G (R6G) at an extraordinarily low concentration of 10^{-15} mol/L, corresponding to an enhancement factor of 1.53×10^8. This substrate has an ultralow detection limit, incurs low processing costs and is simple to prepare; thus, the substrate has significant application potential in the trace analysis field.

Highlights

1. The prepared superhydrophobic and hydrophilic composite structure realizes the enrichment and localization of the object to be measured.
2. The laser-induced periodic surface structures (LIPSS) are combined with the silver-plating process to achieve optimal hotspot regularity and high-density distribution.
3. The LIPSS structure was prepared at the edge of the hydrophilic region, and the coffee ring effect was used to further enrich the tested substance in the hotspot distribution region. A detection limit of R6G 10^{-15} mol/L and an enhancement factor up to 1.53×10^8 were realized.

Keywords Femtosecond laser · Surface-enhanced Raman scattering · Coffee ring effect · Superhydrophobic–hydrophilic surface

✉ Zongwei Xu
zongweixu@tju.edu.cn

[1] State Key Laboratory of Precision Measuring Technology and Instruments, Laboratory of Micro/Nano Manufacturing Technology, Tianjin University, Tianjin 300072, China

[2] Shandong Agricultural Equipment Intelligent Engineering Laboratory, Shandong Provincial Key Laboratory of Horticultural Machinery and Equipment, College of Mechanical and Electronic Engineering, Shandong Agricultural University, Tai'an 827101, China

1 Introduction

Detecting ultralow concentration molecules has been a challenge in research and practical applications, especially in areas related to human health, e.g., food safety testing [1–3], environmental online monitoring [4, 5], and early disease diagnosis [6–9]. Common challenges include low analyte concentrations, high testing demands, and the requirement for rapid results. As a result, detection sensitivity,

Published online: 18 January 2024

cost-effectiveness, and efficiency are stringent demands. Surface-enhanced Raman scattering (SERS), which is a highly sensitive, noninvasive, fast, and label-free detection technology, remains one of the most promising approaches [10–12].

Currently, the two main enhancement mechanisms accepted for SERS are electromagnetic enhancement (EM) [13] and chemical enhancement (CM) [14]. Many studies have improved the detection limit of SERS by manipulating these mechanisms, with EM playing a major role (10^8–10^{10} enhancement) [15]. For example, Sakir et al. employed the seed-mediated growth method to fabricate copper nanostructured substrates, where the substrate achieved a detection limit of 10^{-7} mol/L for Rhodamine 6G (R6G)and exhibited excellent uniformity [16]. In addition, He et al. prepared the three-dimensional (3D) silver microsphere aggregation-induced Raman enhanced scattering and utilized the 3D collaborative interaction to create more hotspots to achieve the quantitative detection of carbendazim in tea [1]. Although they have all achieved good enhancement results, there is still a lot of room for improvement in detection limits.

Recently, efforts have attempted to increase the detection sensitivity via the concentration of analytes, and superhydrophobic surfaces are being targeted because they can reduce the spread of analytes and increase the number of molecules per unit area, which enhances detection sensitivity. Song et al. fabricated a bull's eye structure featuring a superhydrophobic gradient through photolithography, achieving a detection limit of 10^{-15} mol/L for R6G [17], and Song et al. investigated a SERS substrate fabrication method that integrates the nanodendrite gold structure with a superwettable surface. This method achieved a detection sensitivity of 10^{-12} mol/L for R6G and inhibited the formation of coffee rings through the ultra-hydrophilic surface [18]. These methods have achieved remarkable detection results; however, the challenges associated with reducing the complexity and cost of the preparation process limit the widespread use of SERS substrates in practical applications. Thus, it is necessary to adopt a simple and low-cost method to prepare high-sensitivity SERS substrates. Laser processing technology is based on the interaction between light and materials, and it is known for its simplicity, efficiency, and cost-effectiveness. Femtosecond laser pulses, with their exceptionally high peak power and minimal thermal damage, offer significant advantages in micro- and nanostructure fabrication [19]. The femtosecond laser processing technology has played a pivotal role in various research and engineering applications, including surface modification [20], surface micro-structuring [21], and the fabrication of SERS substrates [22].

In this paper, a superhydrophobic–hydrophilic SERS substrate is designed and fabricated using femtosecond laser processing. The designed SERS substrate achieves precise analyte enrichment through modulation of the surface wettability. Combined with laser-induced periodic structures, dense and uniform distribution of hotspots is realized, thereby providing an ultrahigh detection sensitivity of 10^{-15} mol/L. In addition, the distinctive surface morphology contrast between the superhydrophobic and hydrophilic regions enables rapid localization of the boundary of trace areas, which facilitates practical detection. The coffee ring effect (CRE) is leveraged to enhance detection sensitivity. With the advantages of high efficiency, good affordability, and high sensitivity, the proposed superhydrophobic–hydrophilic patterned Cu@Ag composite SERS substrate has great promise as an ultra-sensitive detection technique with application potential in various fields, e.g., food safety and disease diagnosis.

2 Experimental

2.1 Preparation of hybrid Superhydrophobic–Hydrophilic Substrates

A single-sided polished copper sheet (≥ 99.95 wt%; initial size 5 × 5 × 0.5 mm) was used as the substrate. The femtosecond laser used in this study (BWT Tianjin Ltd.) can generate 285 fs pulses at a wavelength of 515 nm, and its output power, repetition frequency, and pulse number are adjustable through software. A schematic diagram of the SERS substrate preparation and detection process is shown in Fig. 1, and the femtosecond laser processing system is shown in Additional file 1: Fig. S1. Prior to femtosecond laser processing, the sample was cleaned ultrasonically in both ethanol and deionized water for five minutes, respectively, to remove surface impurities. The ultrashort laser pulses were focused onto the sample surface through a 40-mm focal length optical lens (MBFCX10609-A), and the intensity distribution of the laser pulse closely followed a Gaussian distribution. Real-time monitoring of the machining process was enabled using a charge-coupled device camera. In the first step, large aspect ratio microcolumn grid arrays were machined by controlling the uniform motion of the stage. A laser fluence of 4.95 J/cm^2, scanning speed of 6 mm/s, scanning interval of 15 μm, and two reciprocating scans were used in our experiment. During the motion, a square area was retained at the center through programming to facilitate the preparation of periodic structures. In the second step, a laser was employed for point-by-point scanning to induce periodic structural patterns within an 80 μm range inward from the untreated central region. The parameters used are as follows: a laser fluence of 0.34 J/cm^2, an interval of 6 μm, and 200 pulses per point. Following the first and second steps, the sample was cleaned using deionized water for five minutes to remove processing residues.

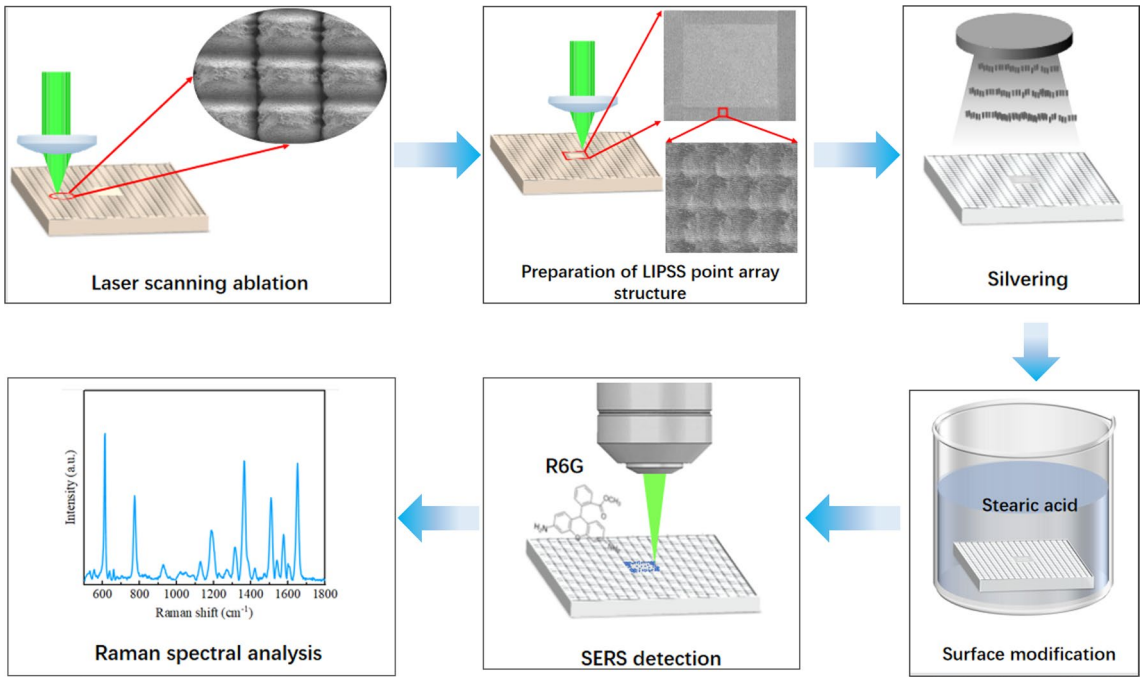

Fig. 1 Schematic diagram of SERS substrate preparation and detection process

In the third step, a layer of silver film (thickness: 80 nm) was deposited on the sample surface using an ion sputtering instrument (ISC150T). In the fourth step, the processed sample was immersed in a 0.01 mol/L stearic acid solution at room temperature for 10 min and left to air dry. In the fifth step, 10 µL liquid drops were added to the SERS substrate using a pipette, and a Raman test was performed after volatilization. Finally, in the sixth step, the measured Raman signals were processed and analyzed. The size of the trace area of the dryer R6G at different immersion times is shown in Additional file 1: Fig. S2.

2.2 Surface Morphology and Hydrophobicity Testing

The surface morphology and trace amounts were characterized using a field emission scanning electron microscope (Apreo S LoVac), a laser scanning confocal microscope (Olympus, OLS4100), an inverted fluorescence microscope (LEICA DMi8), and a commercially available atomic force microscope (AFM, Dimension Icon). The contact angle (CA) measurements of a 10-µL solution of 10^{-7} mol/L R6G were performed using a CA measurement instrument (JC2000D1) under carefully controlled room temperature conditions, ranging from 30.5 to 31.3 °C with a relative humidity of 26.7%–39.1%. To ensure high measurement accuracy and reliability, the measurements were repeated three times, and the averaged results were reported with an error range.

2.3 SERS Spectral Characterization

In Raman testing, a 10-µL R6G solution was dropped onto the substrate surface using a pipette and allowed to air dry at room temperature. Due to the excellent adhesion properties of the central hydrophilic surface, the analytes can be concentrated at specific locations, thereby enhancing SERS performance. The Raman system used in this study comprised a confocal microscope–based smart Raman system (developed by the Institute of Semiconductors, Chinese Academy of Sciences) and a spectrometer (Horiba iHR550) operating at an excitation wavelength of 532 nm. The grating groove density was 600 lines per millimeter (600 gr/mm). Prior to testing, the spectrometer was calibrated carefully using the Raman peak of silicon at 520.7 cm^{-1}. During the measurement, the laser power was approximately 86 µW, the spectral integration time was set to 3 s, the integration was repeated twice, and the spectral range was 500–1800 cm^{-1}. Using a 50× objective lens (Olympus; N.A. = 0.75), the lateral spatial resolution was better than 1 µm, and the axial spatial resolution was better than 2 µm (in air). Given the strong fluorescence peak of R6G at 550 nm [23], baseline correction was performed on the Raman spectra to mitigate its impact on the results.

3 Results and Discussion

3.1 Key Processing Parameters of Superhydrophobic–Hydrophilic Structure

The detailed structures obtained after each processing step are shown in Fig. 2. As can be seen, in Step I, the substrate exhibits a dual-roughness structure [24] comprising a micrometer-scale columnar array generated by laser ablation and nanoscale particles formed through rapid solidification during material removal. These nanoscale particles adhere to the surface and exhibit periodicity. The average spacing between microcolumns is 8.7 μm. In Step II, laser-induced periodic surface structures (LIPSS) with an

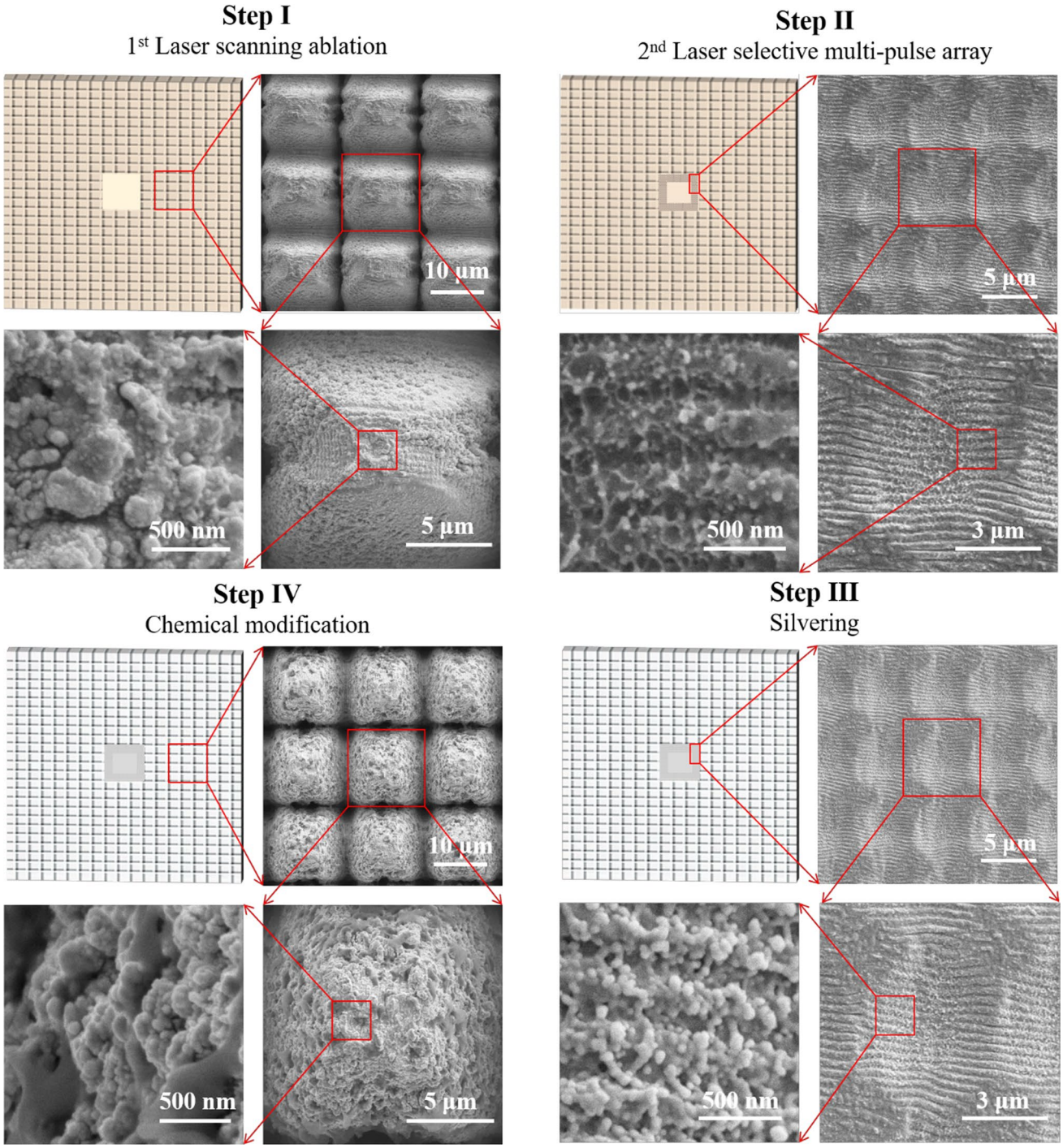

Fig. 2 Fabrication flowchart of hybrid superhydrophobic and hydrophilic platform

average period of 330 nm are generated through laser point array processing. This laser-induced fabrication method produces regular nanoscale periodic structures, which provide an effective and uniform adhesion area for the deposition of the silver film. The formation of periodic nanostructures can be attributed to the interference between the incident laser beam and the surface electromagnetic wave generated at the rough surface [25]. Silver is widely utilized in SERS technology due to its significant enhancement capability. Compared to other enhancing noble metals, e.g., gold and copper, silver is used more extensively to achieve successful SERS [26–28]. By comparing Step II in Fig. 2 with the nanoscale particles, it can be observed that after silver plating, the original nanoscale particles are covered by a silver film, thereby leading to a significant increase in diameter, as shown in Step III (Fig. 2). This silver-plating process results in a closer arrangement of nanoscale particles and a noticeable reduction in particle spacing, which further enhances the SERS effect. For trace detection, the distribution of the analyte on the substrate surface is crucial for the test results. Preparing a superhydrophobic surface reduces the distribution area of trace amounts significantly, thereby increasing the distribution of the analyte within a trace unit area substantially. The hydrophobicity of the material is determined by the surface structure and surface energy; thus, chemical modification of the rough surface is performed using a low surface energy reagent, i.e., stearic acid. The modified substrate exhibits a Cassie–Baxter (CB) state of superhydrophobicity. The final surface morphology of the substrate is shown in Step IV (Fig. 2).

In the CB state, the CA θ_{CB} can be obtained as follows [22]:

$$\cos\theta_{CB} = f(\cos\theta + 1) - 1, \tag{1}$$

where θ and f represent the equilibrium CA of the droplet on a flat surface and the fraction of the liquid–solid contact area, respectively. Based on this formula, reducing the solid–liquid interface area fraction can enhance the surface superhydrophobicity significantly. Increasing the amount of material removed during laser processing can increase the air volume between the liquid droplets and the bottom substrate. Previous studies [29] have demonstrated that the presence of air at the bottom can exert an upward force on the liquid droplets, thereby promoting the CB state. Three types of microcolumn grid arrays were processed by adjusting the laser flux. (1) Type I: under a laser flux of 3.54 J/cm^2, the array's average depth was 11.06 µm, and the average width was 9.57 µm. Here, the CA was 141.3° (Fig. 3a, d, g). Although the CA was improved significantly compared to the untreated surface, it did not achieve the level of superhydrophobicity. (2) Type II: when the laser flux increased to 4.95 J/cm^2, the average depth of the microcolumns reached 13.98 µm with an average width of 9.64 µm. Compared to Type I, the depth increased significantly, and the width remained nearly constant. This occurs due to the fixed size of the focused spot and its Gaussian energy distribution. As the laser flux increases, the energy change primarily concentrates near the center of the spot, which results in a more pronounced depth change, and the width remains relatively constant. At this point, the CA reached 156.3°, thereby satisfying the requirements for superhydrophobicity (Fig. 3b, e, h). (3) Type III: with the continuous increase of laser energy, when the laser flux reaches 6.36 J/cm^2, material removal cannot be discharged promptly, which leads to the accumulation of removed material at the bottom [30, 31] and results in a shallower processing depth. The cross-sectional depth profile reveals the appearance of a distinct small peak at the bottom, which is the redeposition of the removed material. Here, the average depth was 9.38 µm, and the average width was 9.30 µm. At this stage, the CA was only 120° (Fig. 3c, f, i). Thus, the selection of laser flux has a direct effect on the surface hydrophobicity. Among these three groups of results, the hydrophobicity of the Type II substrate was the best, and the processing parameters of the Type II structure were adopted in subsequent investigations.

For SERS detection, the distribution position and area of the analyte are critical for the detection results. Due to the low adhesiveness of superhydrophobic surfaces, the addition of droplets frequently poses challenges, resulting in an inability to fix the distribution position of the analyte on the surface. In addition, influenced by the CRE [32], the distribution of the analyte within the trace area is not uniform (Fig. 4a, d). This nonuniform distribution poses significant challenges for detecting the analyte concentration accurately. During the evaporation process, as the droplet volume decreases, the Laplace pressure [33, 34] ($P_L = 2\gamma_L/R$ given by the Young–Laplace equation, where γ_L is the liquid surface tension, and R is the droplet curvature radius) increases. Increasing the Laplace pressure gradually triggers the wetting state transition from the CB state to the Wenzel state [35], which results in a gradual reduction in CA and stabilization of the contact line (CL). Subsequently, the trace area no longer diminishes. Based on this, a large CA and retractable CL can be achieved through the external superhydrophobic surface by fabricating a superhydrophobic–hydrophilic composite structure. The adsorption of the test droplet relies on the central hydrophilic region, ultimately concentrating the analyte molecules entirely within the hydrophilic area. To minimize the trace area as much as possible, the determination of the hydrophilic region area is of paramount importance. First, the trace area is determined on the superhydrophobic surface. By adding 10 µL of R6G solution on the surface, the trace area was measured as approximately 0.33 mm^2, as shown in Fig. 4a, d,

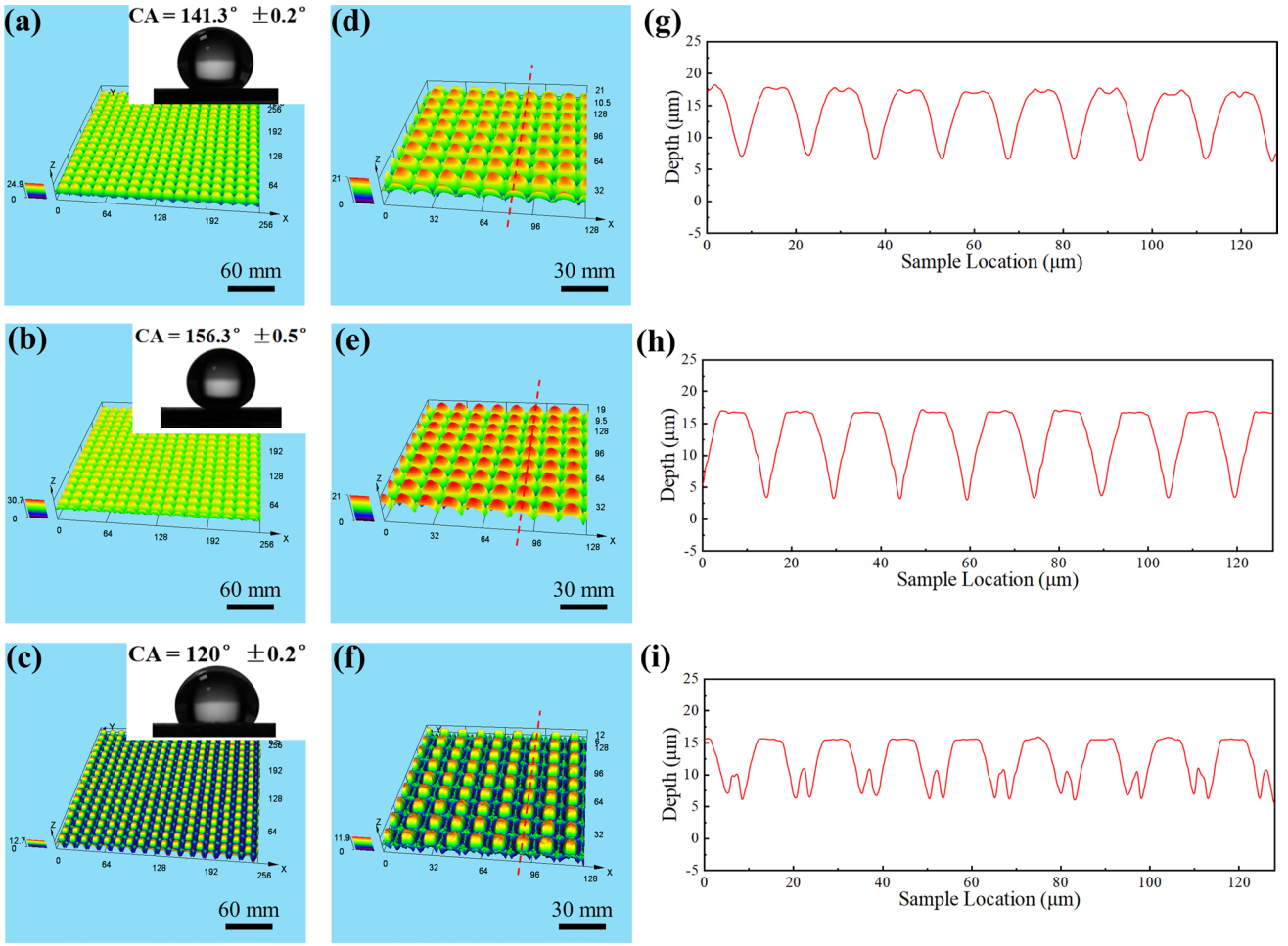

Fig. 3 Surface morphology of superhydrophobic structure under different laser fluxes. 3D surface profiles in (**a**) 3.54 J/cm^2, (**b**) 4.95 J/cm^2 and (**c**) 6.36 J/cm^2. **d–f** Magnified images corresponding to (**a–c**). **g–i** 3D depth profiles at the dashed line positions shown in (**d–f**), respectively

from which the size of the central square unprocessed area shown in Fig. 4b, e can be determined. The distribution of the analyte after drying is shown in Fig. 4b, e. As can be seen, the analyte is well-distributed within the designated area, with significant enrichment of the analyte at the edges of the specified region. Due to the influence of surface tension, the droplet exhibits more pronounced contraction at the four corners of the central square area, thereby ensuring that the edge enrichment region remains within the dot array structure area. This also leads to a more significant accumulation of the test substance at the edge compared to other edge regions (Fig. 4e). Using this approach, the distribution range of the analyte can be determined, and the concentration of the analyte can be further amplified by the CRE. This method is particularly beneficial for detecting colorless analytes or those with extremely low concentrations.

The significant enhancement of SERS occurs exclusively on or near rough metal surfaces, and it operates at the nanoscale level [36]. Thus, employing the femtosecond laser-induced processing method, a dot array structure with nanoscale periodic ripples is created in the hydrophilic region. To enhance processing efficiency, based on the experimental results shown in Fig. 4b, e and the actual size of the detection area, the hydrophilic region is not subjected to overall dot array processing. Instead, processing is applied to the edge regions where a more pronounced enrichment phenomenon is observed to ensure the accumulation and deposition of the test substance on the dot array structure. The distribution of analytes on the substrate after processing is shown in Fig. 4c, f. Remarkably, the dot array structure has no impact on the surface hydrophobicity or the distribution of analytes, which is consistent with the distribution observed prior to processing. In addition, the enrichment of the analyte in the edge region is confined within the dot array structure. Distinct morphological differences between the different structures result in high identification accuracy, thereby enabling rapid localization during the detection processes.

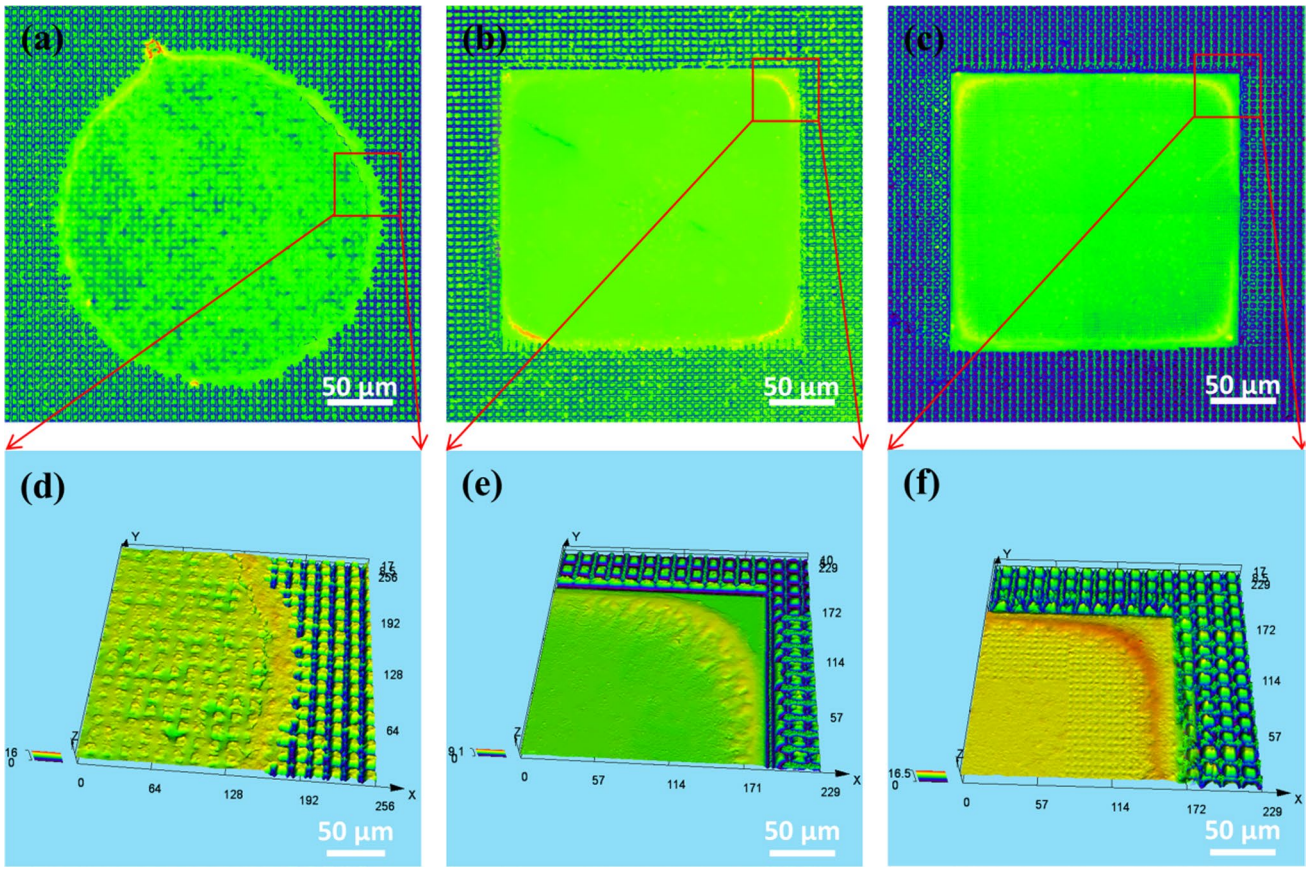

Fig. 4 Traces of area after evaporation of 10 μL 10^{-7} mol/L R6G on different treated surfaces. **a** and **d** show the superhydrophobic surfaces, and **b** and **e** show the superhydrophobic–hydrophilic surfaces (hydrophilic region untreated). **c** and **f** show the superhydrophobic–hydrophilic surfaces (with periodic ripple structures prepared in the hydrophilic region). Note that (**d**–**f**) are localized 3D magnifications corresponding to (**a**–**c**)

Figure 5 shows the morphology of a single point under AFM testing. The surface exhibits a series of uniformly spaced periodic ripples with an average initial spacing of 174.2 nm. To minimize the potential impact of processing depth on the detection results, the maximum processing depth of individually prepared points remains below 600 nm, which is significantly smaller than the longitudinal spatial resolution of approximately 2 μm.

3.2 SERS Substrate Enrichment Capability and Wetting Characteristics Evaluation

Figure 6 shows the evaporation process of the liquid droplets and the deposition morphology of analytes on substrates with different wetting modes, including on bare copper (i.e., only coated with silver) for substrate Types IV and V. Type IV and Type V are improvements based on Type I and Type II, with the structure shown in Fig. 4c prepared in the central region. Figure 6a shows the temporal reduction in the CA of the liquid droplet on the SA-modified silver-coated bare copper surface starting below 90°, which indicates its hydrophilic

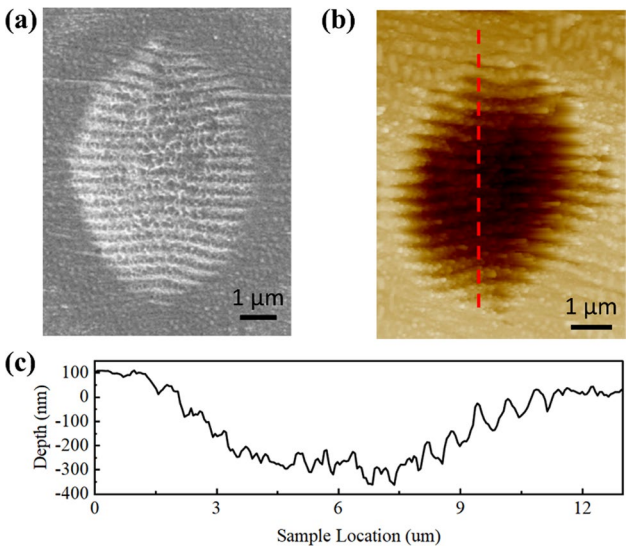

Fig. 5 **a** SEM image of a single-point structure within the dot array structure. **b** AFM image of a single-point structure within the dot array structure. **c** Relevant depth profiles along the marked line

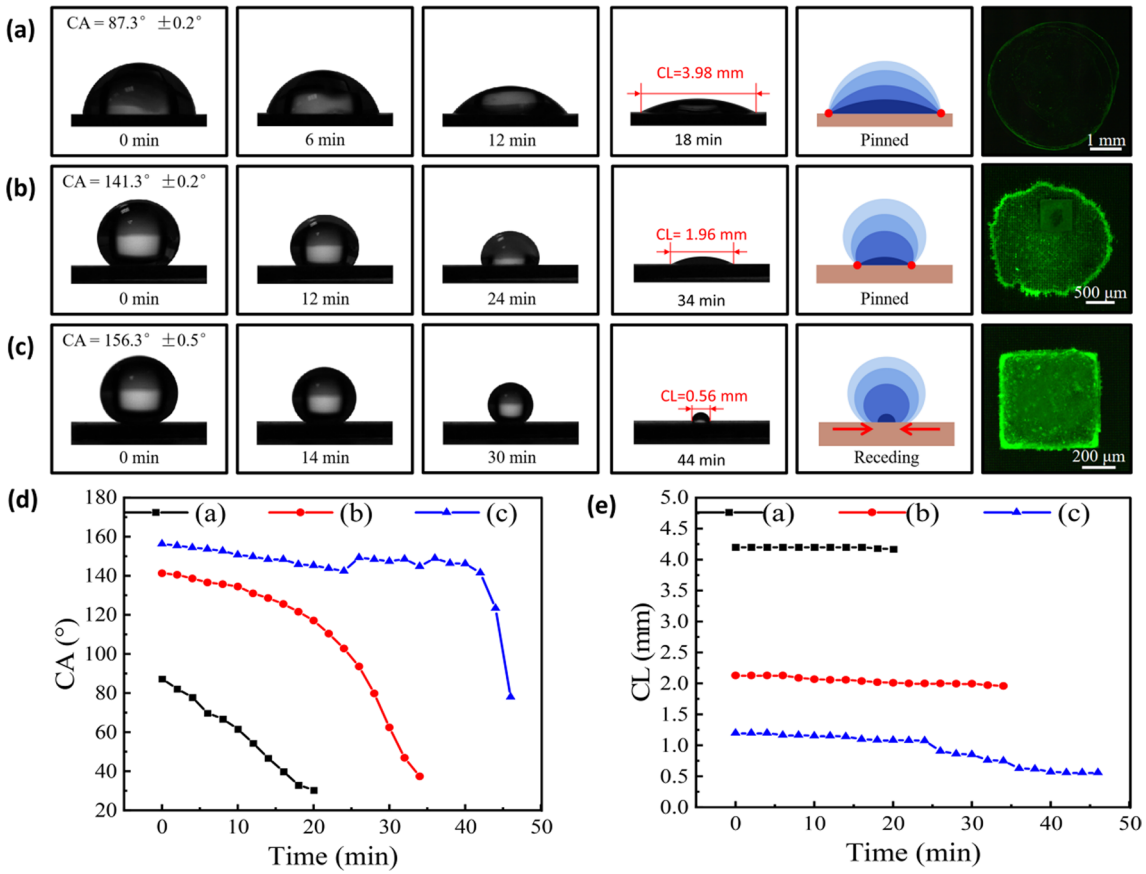

Fig. 6 Evaporation processes of 10 μL drops contain 10^{-7} mol/L R6G on SA-modified, **a** silver-plated copper, **b** Type IV surfaces, and, **c** Type V surfaces. The fluorescence images on the far right in (**a**–**c**) display the distribution of R6G after evaporation. **d** Variation of the CA with the evaporation time. **e** Variation of the CL with the evaporation time

nature. The CL is relatively long and remains nearly fixed on the surface. The rapid evaporation rate at the CL facilitates capillary flow, whereby dispersed nanoparticles are continuously transported toward the droplet edge [37]. Eventually, analytes accumulate along the CL, giving rise to a coffee ring formation with a diameter of 3.98 mm, which corresponds to an area of 12.43 mm^2. The initial length of the CL at the same droplet volume relies on the CA, where a larger CA corresponds to a shorter initial CL. The Type IV substrate exhibits high adhesion and hydrophobicity (Fig. 6b), with an initial CA of 141.3° and a CL length of 1.96 mm. The area of deposited analytes is reduced by 4.1 times compared to that on the bare surface. However, due to its high adhesion, the CL is not shortened significantly during the entire evaporation process. On the Type V low-adhesion superhydrophobic surface (Fig. 6c), the initial droplet possesses a larger CA and a shorter CL, and it exhibits low surface adhesion. During the first 44 min of the evaporation process, the CL was shortened continuously. Subsequently, the edge of the droplet coincides with the edge of the square hydrophilic region. The final area of the deposited analytes is 0.31 mm^2, representing a reduction of 40.1 times compared to the bare surface. The fluorescence images in Fig. 6a–c show the distribution of the test substance after the droplet has evaporated. For the Type V substrates, even if the droplet release position is slightly offset from the center region, the added droplets are anchored to the central area, ultimately fixing the trace area in the center region. Figure 6d, e shows detailed plots of the corresponding changes in CA and CL over the course of the evaporation process. Compared with the bare copper (only coated with silver) and Type IV substrates, the CA of droplets on the Type V substrate remains stable for a longer period, and the CL has an obvious contraction, with the final CL being only half of the initial CL.

3.3 Detection Limits and Uniformity at Different Silver Deposition Thicknesses

The prominent Raman peak of R6G in the spectrum is labeled in Fig. 7a. Here, the peaks at 611 and 772 cm^{-1} correspond to the in-plane bending of the C–C–C ring and the out-of-plane bending of the C–H bonds, respectively. The peaks observed at 1181, 1368, 1506, 1576 and 1654 cm^{-1} are

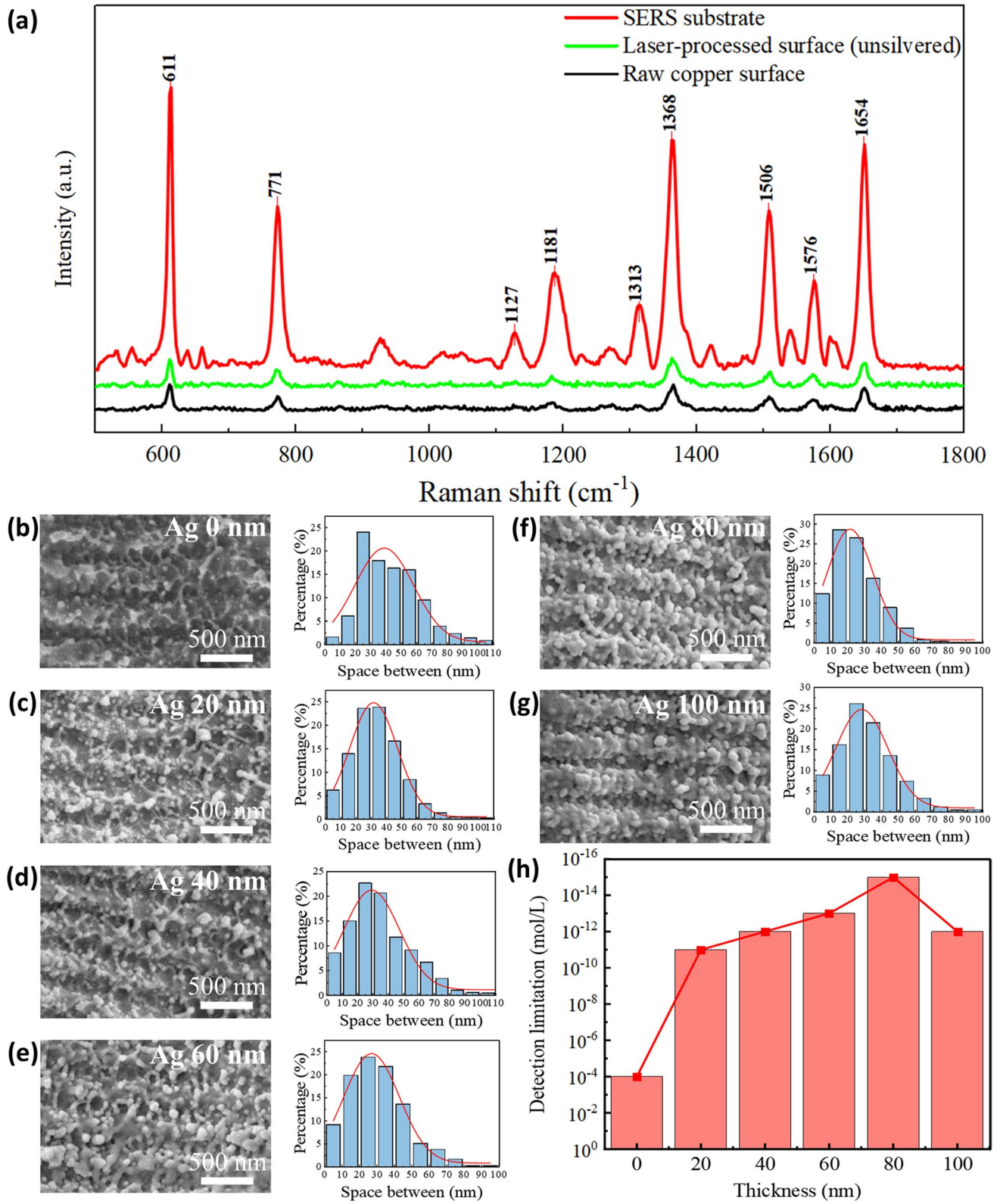

Fig. 7 **a** Raman signals of R6G on the raw copper surface, the laser-processed surface (unsilvered) (10^{-4} mol/L), and the SERS substrate (10^{-7} mol/L). **b**–**g** SEM images of silver deposition thickness ranging from 0 to 100 nm with histograms showing the distribution of proportions in intervals. **h** Detection limits of R6G at different silver deposition thicknesses

associated with the C–C stretching vibrations related to the benzene ring. In addition, the peak at 1127 cm^{-1} is related to the in-plane C–H bending vibrations associated with the benzene ring, and the peak at 1313 cm^{-1} is classified as C–H bending vibrations related to the benzene ring [26, 38]. Figure 7a shows the Raman detection results for R6G at concentrations of 10^{-4} mol/L on the raw copper surface and the laser-processed surface (unsilvered) and 10^{-7} mol/L on the fabricated SERS substrate. On the raw copper surface, the lowest detectable concentration of R6G is 10^{-4} mol/L. The detection effect of the copper surface processed by the laser is essentially the same as that of the unprocessed copper surface because the enhancement effect of copper is weak, and the resulting copper nanoparticles are oxidized and lose the enhancement effect due to processing in air. To improve the enhancement effect of the prepared substrate, the silver film is plated on the surface of the copper after laser processing. Figure 7b–g exhibits SEM images presenting various silver-plated thicknesses accompanied by histograms showing the ratios of nanoparticle spacing. With the augmentation of silver-plated thickness, the nanoparticle size increases, concomitant with a reduction in interparticle separation. As the spacing between the silver nanoparticles decreases, the enhancement effect of the hotspots becomes increasingly pronounced [39]. Here, a hotspot refers to extremely close gaps between nanostructured materials where the electromagnetic field experiences significant enhancement, thereby leading to substantial SERS enhancement [13]. Prior to silver plating, the spacing between the nanoparticles primarily ranges from 20 to 80 nm. With the increase in silver-plating thickness, when the thickness reaches 80 nm, the nanoparticle spacing decreases noticeably, primarily falling within the range of 0–40 nm, which is preferable in SERS detection. The substantial rise in the proportion of spacing within the intervals of 0–10 nm and 10–20 nm is particularly noteworthy. In addition, as the silver thickness continues to increase, noticeable nanoparticle fusion occurs, which results in a weakening of the SERS enhancement effect. By testing the detection limits of substrates with different silver-plating thicknesses, the test results are consistent with the trend of the nanoparticle spacing interval proportions. In the range of 0–80 nm, the proportion of nanoparticle spacing within the smaller intervals gradually rises as the silver-plating thickness increases, thereby resulting in a significant enhancement of the substrate detection sensitivity. Nevertheless, at a silver-plating thickness of 100 nm, the proportion of nanoparticle spacing within the smaller intervals decreases compared to the 80 nm cases, which results in a reduction in detection sensitivity. This trend is shown in Fig. 7h.

In SERS applications, the detection limit is an important parameter to evaluate the practicability of a SERS substrate. To investigate the detection limit of the prepared substrate, R6G solutions of different concentrations were prepared for Raman spectroscopy measurements. Figure 8a–c shows SEM images of the dot array structure region after evaporation. The nanoparticles on the substrate are enveloped by R6G, leading to a significant enhancement of the electromagnetic field [40]. Figure 8d, e shows the R6G Raman signal from 10^{-7} to 10^{-15} mol/L on the substrate. As can be seen, significant Raman peaks are observed at 611, 771, 1181, 1368, 1506 and 1654 cm^{-1}, even though the R6G concentration is as low as 10^{-15} mol/L. In determining the analyte, the more characteristic Raman peaks there are, the more accurately the analyte can be identified. This indicates that the prepared SERS substrate can detect extremely low analyte concentrations. According to the Raman intensity of 10^{-15} mol/L at 611 cm^{-1} and the Raman peak intensity of 10^{-4} mol/L R6G on the original copper surface, the corresponding enhancement factor (EF) can be calculated as follows [41].

$$\mathrm{EF} = \frac{I_{\mathrm{SERS}}/N_{\mathrm{SERS}}}{I_{\mathrm{Ref}}/N_{\mathrm{Ref}}} \tag{2}$$

Here, I_{SERS} and I_{Ref} represent the Raman signal intensity collected from the SERS substrate and raw copper surface, respectively, and N_{SERS} and N_{Ref} are the number of molecules adsorbed per unit area on the SERS substrate and raw copper surface, respectively. The calculated EF is approximately 1.53×10^8 (additional details are provided in the Supporting Information).

In addition, the uniformity and consistency of the dot array structure in the prepared substrate were also examined, as shown in Fig. 8f, g. Calculations reveal that, even at a low concentration of 10^{-11} mol/L, the relative standard deviation of the Raman signal at 611 cm^{-1} remains remarkably low at 11.9%. The distribution of the peak intensities between two neighboring processing points within the processing area is nearly identical. Thus, we confirm that the processed dot array structure demonstrates excellent uniformity and consistency.

4 Conclusion

This study developed a superhydrophobic–hydrophilic patterned Cu@Ag SERS substrate using a femtosecond laser to realize highly sensitive analyte detection. By adjusting the laser flux combined with surface modification, the prepared superhydrophobic–hydrophilic composite structure enables the enrichment and localization of the analyte. An optimized superhydrophobic structure was achieved using a laser flux of 4.95 J/cm^2. Under different silver-plating thicknesses, the spacing between the silver-plated nanoparticles on the induced periodic structure was compared, and the optimal preparation of the local hotspot enhancement

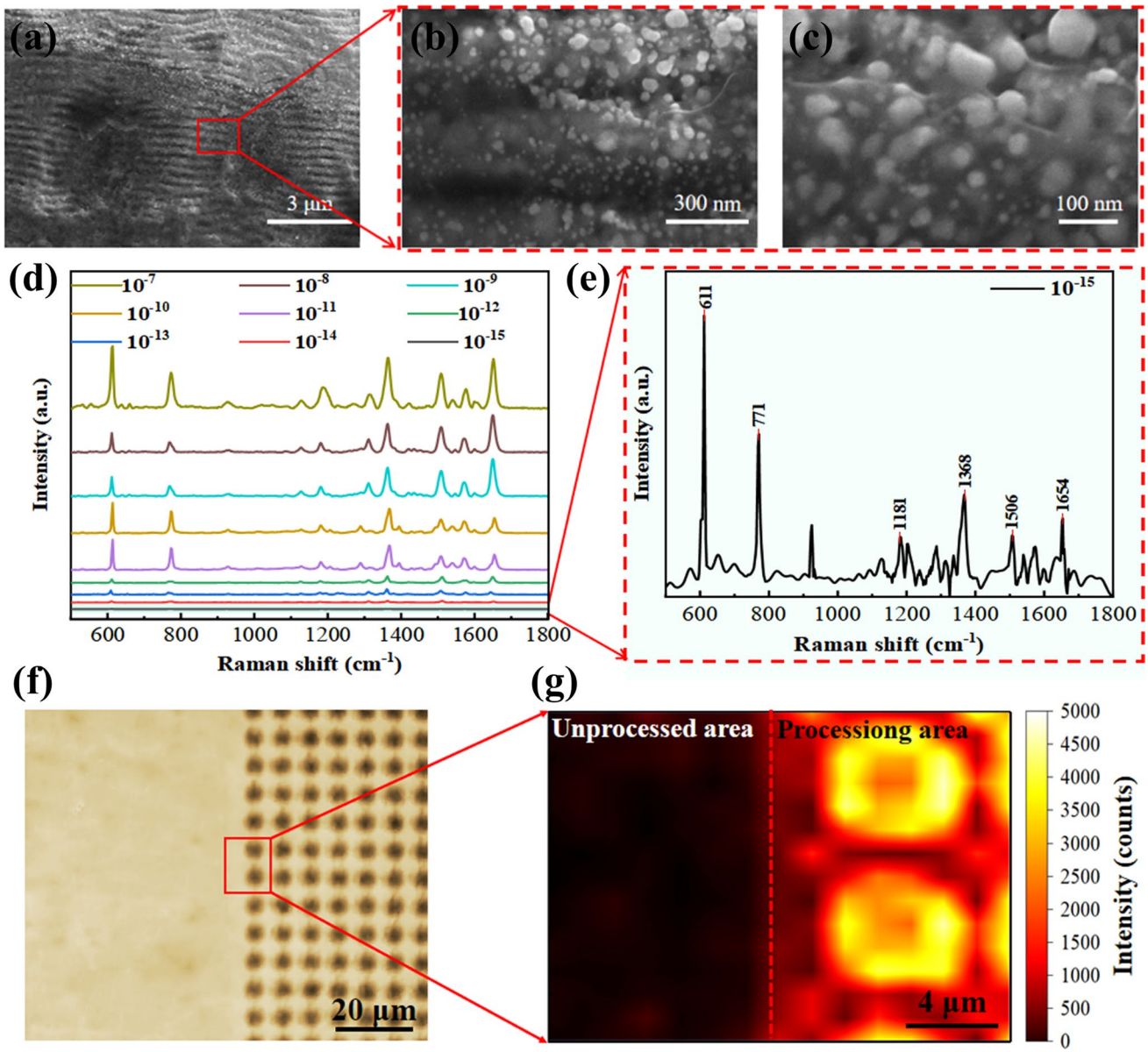

Fig. 8 **a** SEM images of R6G deposited on a periodically striped structure after evaporation. **b**, **c** show magnified views of (**a**). **d**, **e** Raman spectra of R6G with different concentrations. **f** Microscopic imaging under the Raman platform (after evaporation of 10 μL of 10^{-11} mol/L R6G). **g** Raman intensity mapping (611 cm^{-1}) of the marked area in (**f**)

effect generated by the nanoscale periodic fringe structure was accomplished with a silver-plating thickness of 80 nm. Affected by the CRE, the analyte accumulates significantly at the edges of the hydrophilic region. Under the influence of surface tension, the four corners of the square hydrophilic region experience further accumulation compared to the other edges. Leveraging the morphological difference between the superhydrophobic and hydrophilic regions allows for rapid and accurate positioning of the four corners of the hydrophilic region, thereby maximizing the utilization of the CRE and achieving the highest possible detection sensitivity. The lowest detection limit of the prepared SERS substrate is 10^{-15} mol/L, and the EF is as high as 1.53×10^8. In addition, the matrix structure of the substrate exhibits good uniformity and consistency, which guarantees the reliability of practical applications. This highly sensitive SERS substrate is expected to serve as a powerful tool for molecular detection, presenting wide ranging application potential in various fields, e.g., food safety, environmental monitoring, and disease diagnosis.

Supplementary Information The online version contains supplementary material available at https://doi.org/10.1007/s41871-024-00222-z.

Acknowledgements The authors gratefully acknowledge support from National Natural Science Foundation of China (Nos. 52035009, 51761135106), 2020 Mobility Programme of the Sino-German Center for Research Promotion (M-0396), and the '111' project by the State Administration Foreign Experts Affairs and the Ministry of Education of China (Grant No.B07014).

Author contributions All authors read and approved the final manuscript.

Availability of Data and Materials The authors declare that all data supporting the findings of this study are available within the article.

Declarations

Competing interests The authors declare that they have no conflicts of interest.

References

1. He J, Li H, Zhang L, Zhi X et al (2021) Silver microspheres aggregation-induced Raman enhanced scattering used for rapid detection of carbendazim in Chinese tea. Food Chem 339:128085. https://doi.org/10.1016/j.foodchem.2020.128085
2. Hajikhani M, Zhang Y, Gao X et al (2023) Advances in CRISPR-based SERS detection of food contaminants: a review. Trends Food Sci Tech 138:615–627. https://doi.org/10.1016/j.tifs.2023.07.001
3. Xiong S, He T, Zhou T et al (2022) In situ synthesis of MXene/Ag nanocomposites based flexible SERS substrates on PDMS for detection on fruit surfaces. Colloid Surface A 654:130077. https://doi.org/10.1016/j.colsurfa.2022.130077
4. Phuong NTT, Nguyen T-A, Huong VT et al (2022) Sensors for detection of the synthetic dye rhodamine in environmental monitoring based on SERS. Micromachines 13:1840. https://doi.org/10.3390/mi13111840
5. Chio W-IK, Xie H, Zhang Y et al (2022) SERS biosensors based on cucurbituril-mediated nanoaggregates for wastewater-based epidemiology. TrAC Trends Anal Chem 146:116485. https://doi.org/10.1016/j.trac.2021.116485
6. Chen Y, Zheng S, Tang X et al (2023) Recent research progress of surface enhanced Raman scattering dominated analysis strategy in early diagnosis of diseases. Chem-Asian J 18:e202300264. https://doi.org/10.1002/asia.202300264
7. Guerrini L, Garcia-Rico E, O'Loghlen A et al (2021) Surface-enhanced Raman scattering (SERS) spectroscopy for sensing and characterization of exosomes in cancer diagnosis. Cancers 13:2179. https://doi.org/10.3390/cancers13092179
8. Yu D, Yin Q, Wang J et al (2021) SERS-based immunoassay enhanced with silver probe for selective separation and detection of Alzheimer's disease biomarkers. Int J Nanomed 16:1901–1911. https://doi.org/10.2147/IJN.S293042
9. Xiang S, Lu L, Zhong H et al (2021) SERS diagnosis of liver fibrosis in the early stage based on gold nanostar liver targeting tags. Biomater Sci 9:5035–5044. https://doi.org/10.1039/d1bm00013f
10. Sun Y, Chen X, Zheng Y et al (2020) Surface-Enhanced Raman scattering trace-detection platform based on continuous-rolling-assisted evaporation on superhydrophobic surfaces. ACS Appl Nano Mater 3:4767–4776. https://doi.org/10.1021/acsanm.0c00745
11. Bharati MSS, Soma VR (2021) Flexible SERS substrates for hazardous materials detection: recent advances. Opto-Electron Adv 4:210048–210048. https://doi.org/10.29026/oea.2021.210048
12. Ma X, Jiang L, Li X et al (2019) Hybrid superhydrophilic–superhydrophobic micro/nanostructures fabricated by femtosecond laser-induced forward transfer for sub-femtomolar Raman detection. Microsyst Nanoeng 5:48. https://doi.org/10.1038/s41378-019-0090-1
13. Ding S, You E, Tian Z et al (2017) Electromagnetic theories of surface-enhanced Raman spectroscopy. Chem Soc Rev 46:4042–4076. https://doi.org/10.1039/c7cs00238f
14. Itoh T, Procházka M, Dong Z et al (2023) Toward a new era of SERS and TERS at the nanometer scale: from fundamentals to innovative applications. Chem Rev 123:1552–1634. https://doi.org/10.1021/acs.chemrev.2c00316
15. Luo X, Pan R, Cai M, Liu W et al (2021) Atto-Molar Raman detection on patterned superhydrophilic-superhydrophobic platform via localizable evaporation enrichment. Sens Actuators B 326:128826. https://doi.org/10.1016/j.snb.2020.128826
16. Sakir M, Yilmaz E, Onses MS (2020) SERS-active hydrophobic substrates fabricated by surface growth of Cu nanostructures. Microchem J 154:104628. https://doi.org/10.1016/j.microc.2020.104628
17. Song W, Psaltis D, Crozier KB (2014) Superhydrophobic bull's-eye for surface-enhanced Raman scattering. Lab Chip 14:3907–3911. https://doi.org/10.1039/c4lc00477a
18. Song Y, Xu T, Xu L-P et al (2018) Superwettable nanodendritic gold substrates for direct miRNA SERS detection. Nanoscale 10:20990–20994. https://doi.org/10.1039/c8nr07348a
19. Ding K, Wang C, Zheng Y et al (2019) One-step fabrication of multifunctional fusiform hierarchical micro/nanostructures on copper by femtosecond laser. Surf Coat Technol 367:244–251. https://doi.org/10.1016/j.surfcoat.2019.04.005
20. Yong J, Huo J, Yang Q et al (2018) Femtosecond laser direct writing of porous network microstructures for fabricating super-slippery surfaces with excellent liquid repellence and anti-cell proliferation. Adv Mater Interfaces 5:1701479. https://doi.org/10.1002/admi.201701479
21. Sun K, Yang H, Xue W et al (2018) Tunable bubble assembling on a hybrid superhydrophobic–superhydrophilic surface fabricated by selective laser texturing. Langmuir 34:13203–13209. https://doi.org/10.1021/acs.langmuir.8b02879
22. Luo X, Liu W, Chen C et al (2021) Femtosecond laser micro-nano structured Ag SERS substrates with unique sensitivity, uniformity and stability for food safety evaluation. Opt Laser Technol 139:106969. https://doi.org/10.1016/j.optlastec.2021.106969
23. Verma VK, Tapadia K, Maharana T et al (2018) Convenient and ultra-sensitive fluorescence detection of bovine serum albumin by using Rhodamine-6G modified gold nanoparticles in biological samples. Luminescence 33:1408–1414. https://doi.org/10.1002/bio.3563

24. Parvate S, Dixit P, Chattopadhyay S (2020) Superhydrophobic surfaces: insights from theory and experiment. J Phys Chem B 124:1323–1360. https://doi.org/10.1021/acs.jpcb.9b08567
25. Sipe JE, Young JF, Preston JS et al (1983) Laser-induced periodic surface structure. I. Theory. Phys Rev B 27:1141–1154. https://doi.org/10.1103/PhysRevB.27.1141
26. Chang T, Chang Y, Chen C et al (2019) A facile method to directly deposit the large-scale Ag nanoparticles on a silicon substrate for sensitive, uniform, reproducible and stable SERS substrate. J Alloy Compd 782:887–892. https://doi.org/10.1016/j.jallcom.2018.12.264
27. Zhang H, Wang J, Li G et al (2019) Fabrication of Ag-nanosheet-assembled hollow tubular array and their SERS effect. J Alloy Compd 772:663–668. https://doi.org/10.1016/j.jallcom.2018.09.130
28. Wang X, Liu X, Li F et al (2023) Multifunctional 3D magnetic carbon aerogel for adsorption separation and highly sensitive SERS detection of malachite green. Chemosphere 339:139654. https://doi.org/10.1016/j.chemosphere.2023.139654
29. Wang L, Tian Z, Luo X et al (2022) Superomniphobic surfaces for easy-removals of environmental-related liquids after icing and melting. Nano Res 16:3267–3277. https://doi.org/10.1007/s12274-022-4887-2
30. Liu H, Li Y, Lin W et al (2020) High-aspect-ratio crack-free microstructures fabrication on sapphire by femtosecond laser ablation. Opt Laser Technol 132:106472. https://doi.org/10.1016/j.optlastec.2020.106472
31. Zhang K, Xu Z, Dong B et al (2023) Process exploration of β-Ga_2O_3 blind hole processing by water-assisted femtosecond laser technology. J Alloy Compd 939:168769. https://doi.org/10.1016/j.jallcom.2023.168769
32. Hu H, Larson RG (2002) Evaporation of a sessile droplet on a substrate. J Phys Chem B 106:1334–1344. https://doi.org/10.1021/jp0118322
33. Annavarapu RK, Kim S, Wang M et al (2019) Explaining evaporation-triggered wetting transition using local force balance model and contact line-fraction. Sci Rep 9:405. https://doi.org/10.1038/s41598-018-37093-6
34. Han J, Cai M, Lin Y et al (2018) Comprehensively durable superhydrophobic metallic hierarchical surfaces via tunable micro-cone design to protect functional nanostructures. RSC Adv 8:6733–6744. https://doi.org/10.1039/c7ra13496g
35. Gao Y, Yang N, You T et al (2018) Superhydrophobic "wash free" 3D nanoneedle array for rapid, recyclable and sensitive SERS sensing in real environment. Sens Actuat B-Chem 267:129–135. https://doi.org/10.1016/j.snb.2018.04.025
36. Jeanmaire DL, Van Duyne RP (1977) Surface Raman spectroelectrochemistry: part I. Heterocyclic, aromatic, and aliphatic amines adsorbed on the anodized silver electrode. J Electroanal Chem Interfacial Electrochem 84:1–20. https://doi.org/10.1016/S0022-0728(77)80224-6
37. He A, Yang H, Xue W et al (2017) Tunable coffee-ring effect on a superhydrophobic surface. Opt Lett 42:3936–3939. https://doi.org/10.1364/ol.42.003936
38. Syed H et al (2015) SERS studies of explosive molecules with diverse copper nanostructures fabricated using ultrafast laser ablation. Adv Mater Lett 6:1073–1080. https://doi.org/10.5185/amlett.2015.6007
39. Meng W, Hu F, Jiang X et al (2015) Preparation of silver colloids with improved uniformity and stable surface-enhanced Raman scattering. Nanoscale Res Lett 10:1–8. https://doi.org/10.1186/s11671-015-0746-1
40. Huang Y, Chen Y, Xue X et al (2018) Unexpected large nanoparticle size of single dimer hotspot systems for broadband SERS enhancement. Opt Lett 43:2332–2335. https://doi.org/10.1364/ol.43.002332
41. Rui Tan JM, Ruan JJ, Lee HK et al (2014) A large-scale superhydrophobic surface-enhanced Raman scattering (SERS) platform fabricated via capillary force lithography and assembly of Ag nanocubes for ultratrace molecular sensing. Phys Chem Chem Phys 16:26983–26990. https://doi.org/10.1039/c4cp03679d

Yuheng Zhang State Key Laboratory of Precision Measuring Technology and Instruments, School of Precision Instruments and Opto-Electronics Engineering, Tianjin University, China, is studying for master's degree. His research interests include ultra-fast femtosecond laser processing, Raman spectroscopy and SERS substrate preparation.

Zongwei Xu is the Professor of Tianjin University, Doctoral Supervisor. His research interests include: ultra-fast energy beam (ion, laser) processing, Raman and photoluminescence spectroscopy characterization, wide bandgap semiconductor devices, microcutting tool and nanocutting technology. He is the Chairman of the first Sino-German symposium of "Defect Engineering in SiC Device Manufacturing - Atomistic Simulations, Characterization and Processing" and the Principle Investigator of 2021–2023 Mobility Programme of the Sino-German Center for Research Promotion (M-0396).

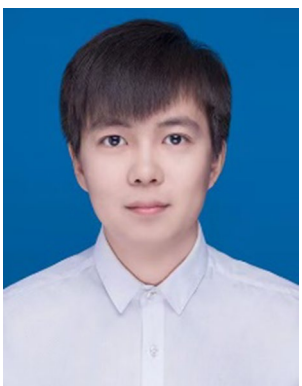

Kun Zhang College of Mechanical and Electronic Engineering, Shandong Agricultural University, Taian 271018, China, studied at Tianjin University for a PhD. His research interests cover the application of ultra-fast femtosecond laser processing, Raman spectroscopy, fluorescence spectroscopy and other technologies in ultra-wide band gap semiconductor materials gallium oxide.

Ying Song State Key Laboratory of Precision Measuring Technology and Instruments, School of Precision Instruments and Opto-Electronics Engineering, Tianjin University, China, is studying for PhD degree. Her research interests include preparation of silicon carbide color centers by ion implantation, three-dimensional Raman and photoluminescence spectral characterization, and model of spectral depth profiling.

Bing Dong State Key Laboratory of Precision Measuring Technology and Instruments, School of Precision Instrument and Opto-Electronics Engineering, Tianjin University, China, is studying for Doctor's degree.

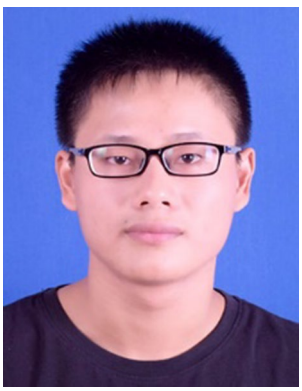

Jianshi Wang State Key Laboratory of Precision Measuring Technology and Instruments, School of Precision Instruments and Opto-Electronics Engineering, Tianjin University, China, is studying for master's degree. His research interests include ultrafast femtosecond laser processing, Raman spectroscopy and nanoparticle fabrication.

Mengzhi Yan State Key Laboratory of Precision Measuring Technology and Instruments, School of Precision Instruments and Opto-Electronics Engineering, Tianjin University, China, is studying for master's degree. His research interests include heuristic algorithm, MD simulation and detecting defects in ultra-wide band gap semiconductor material, gallium oxide by machine learning.

Qingqing Sun State Key Laboratory of Precision Measuring Technology and Instruments. School of Precision Instrument and Opto-Electronics Engineering, Tianjin University, China, is studying for master's degree.